Flush-mounted Langmuir probes in the WEST tokamak divertor

R. Dejarnac[a,*], D. Sestak[a], J. P. Gunn[b], M. Firdaouss[b], H. Greuner[c], J-Y. Pascal[b], M. Richou[b], H. Roche[b]

[a]*Institute of Plasma Physics, Czech Academy of Sciences, 182 00 Prague, Czech Republic*
[b]*CEA, IRFM, F-13108 Saint-Paul-lez-Durance, France*
[c]*Max Planck Institute for Plasma Physics, Boltzmannstraße 2, 85748, Garching, Germany*

[*]*corresponding author: Renaud Dejarnac dejarnac@ipp.cas.cz*

Abstract

The design of the Langmuir probes for the lower divertor of the WEST tokamak is presented, in which uncooled, tungsten-coated graphite targets were installed for the first phase of operation in anticipation of full-tungsten, actively cooled, ITER-like divertor components. Due to the long plasma discharges and high heat loads, the probe tips are flush with the divertor tiles in which they are embedded, as it is foreseen and indeed required in ITER. Tantalum metal was chosen for the probe tips because of its high melting point, and ductility at room temperature which allows simple crimping to electrically connect them to cables, as well as being compatible with the full metal environment of WEST. High heat flux tests of Ta Langmuir probe prototypes confirmed the robustness of the design for energy flux densities up to 8 MW/m^2 for 5.5 s, and at lower 3.5 MW/m² energy flux density for 40 s long discharges. The probes were operational from the first discharge in WEST and the good alignment of all probes with the surrounding surface was confirmed by a good match of each adjacent probe's data when the strike points were swept across the target.

1 Introduction

The Tore Supra tokamak [1] went through a major upgrade from being a carbon machine with a toroidal limiter and circular plasma cross section, to a full metal, X-point divertor machine with D-shaped plasma: the tungsten (W) Environment in Steady-state Tokamak (WEST). One of the main goals of this long pulse superconducting tokamak is to test and qualify a full tungsten divertor with ITER-like plasma-facing components under high heat fluxes up to 10 MW/m^2 [2]. Monitoring of the deposited energy is possible using instrumentation such as thermo-couples, calorimetry, fibre Bragg gratings [3,4], and high resolution infrared thermography [5]. However, such diagnostics cannot resolve the local plasma parameters, from which the heat load can also be derived, such as the electron temperature (T_e), density (n_e), and floating potential (V_{fl}). These parameters represent valuable boundary conditions at the target plates for validating modeling efforts and improving understanding of scrape-off layer (SOL) transport and divertor physics such as power deposition, W erosion, local recycling, detachment, or currents circulating in the SOL.

The best method to characterize the plasma parameters in the vicinity of the separatrix strike points on the divertor target is to install Langmuir probes (LP) within the plasma-facing units (PFU) that compose the divertor. The long discharge duration and the expected high heat flux in WEST impose that the LPs must be flush with the PFU surface within which they are

embedded, in order to maximize their chance of survival. The probes are subjected to the same harsh conditions as the divertor itself, but can only be cooled by indirect contact with the targets via heat conduction through an electrical insulator and to a lesser degree via thermal radiation. This is the reason why the International Thermonuclear Experimental Reactor (ITER) LPs are foreseen to be flush-mounted [6,7,8], despite the well-known difficulty of interpreting their current-voltage (*I*-*V*) characteristics [9,10,11,12].

Due to the grazing incidence of the magnetic field with the divertor targets, the geometrical projection of the probe surface area along the field lines can be comparable to both the Debye length and the ion Larmor radius. The ion branch of the *I*-*V* characteristic is dominated by sheath expansion and does not saturate. Two dimensional kinetic modelling of ion collection by flush-mounted probes in magnetized plasmas has provided a basis for interpreting experimental data [13,14], although no independent verification by comparison with independent measurements has been made. An alternative method, known as short circuit ion current theory, that does not require quantitative understanding of the sheath expansion current was proposed [15,16]. When the applied probe voltage is zero with respect to the divertor, i.e., grounded, the sheath is unperturbed by the probe which can be considered as a simple surface element. In that special case, the probe collection area is determined by the simple geometrical projection of its surface along the field lines. If the floating potential is not more negative than $\sim T_e$, the ion branch can be extrapolated back to V=0 providing a reasonably accurate estimate of the ion current density. Comparison of flush-mounted probe data using the short circuit ion current theory with Thomson scattering measurements in DIII-D resulted in good agreement [17]. There is thus an experimental basis to suggest that flush-mounted probes can give quantitatively correct measurements. One of the main goals of the WEST flush-mounted probe project is investigate flush-mounted probe operation in a wide range of operating conditions and provide feedback in anticipation of ITER.

The WEST divertor consists of a single flat target and is divided into 12 sectors each composed of 38 poloidally-running PFUs with width varying between 26 and 31 mm in the toroidal direction. The toroidal width varies poloidally because the divertor is tilted in the poloidal plane, and thus its nominal plasma-facing surface is conical. The phase I divertor, in operation since 2017, is mostly composed of uncooled W-coated, graphite PFUs with 1^o toroidal bevels to protect poloidal leading edges [18]. A dozen of ITER-like actively cooled PFUs composed of W monoblocks (MB), identical to ITER ones in size and technology (with a cooling pipe in the center and a CuCrZr interface), completes the rest of the divertor [19]. Two special, wider uncooled W-coated PFUs host two flush-mounted LP arrays, covering the entire divertor region from high-field side (HFS) to low-field side (LFS) at two different toroidal locations to study the effect of WEST's large toroidal magnetic field ripple [20]. The LP design is described in Section 2, in particular, the predicted WEST plasma scenarios, calculated using 3D test particle simulations, used for designing the probes (Section 2.1), the integration of the probes into the PFUs (Section 2.2), and results from high heat flux tests performed in the neutral beam facility GLADIS at IPP Garching [21] (Section 2.3). Experimental results obtained during the 2019 experimental campaign are presented in Section 3. The summary and conclusions are put together in Section 4.

2 The WEST divertor flush-mounted probes

2.1 Probe design based on predicted WEST plasma scenarios

The divertor LP system was designed and dimensioned before the first plasma in WEST and was based on perpendicular heat fluxes calculated by 3D test particle simulations using a code that was previously applied to the Tore Supra ergodic divertor [22]. Expected scenarios were simulated for different plasma currents (I_p), power in the SOL (P_{SOL}), heat flux decay lengths (λ_q), and X-point heights. The power in the SOL is adjusted to have the targeted 10 MW/m^2 at the outer strike point, assuming zero dissipation. Test particles are injected inside the confined plasma with a Maxwellian distribution having an ion temperature T_i=100 eV and a parallel drift Mach number $M_{//}$=0.2 [23] in order to yield asymmetric heat flux profiles in the ratio 1/3 to 2/3 at the HFS and LFS, respectively, as is generally observed in tokamaks. The particles follow field lines while diffusing radially. The diffusion coefficient is set to $D_\perp$=1.0 m^{2}s^{-1} so as to result in an expected heat flux decay length of λ_q~5 mm at the outboard midplane [24]. We present here two cases corresponding to the candidate standard scenarios: I_p = 500 kA with an X-point height of 90 mm above the flat, open divertor (referred as 'far X-point configuration' further in the text), and I_p = 800 kA with an X-point height of 30 mm (referred as 'near X-point configuration' further in the text). The predicted heat flux profiles in the divertor are shown in Figure 1.

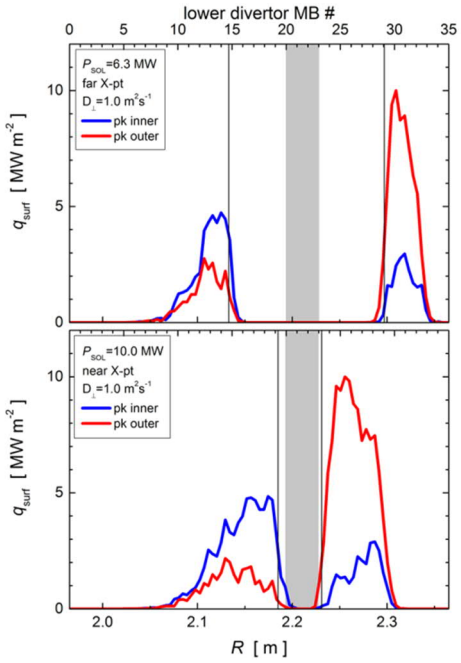

Figure 1. Predicted heat flux profiles in the divertor of WEST calculated by 3D test particle simulations for far X-point (top) and near X-point (bottom) magnetic configurations. The gray shading indicates the region where the graphite PFUs are unshaped, at the transition between inner and outer divertor target zones. The profiles are shown at two toroidal positions separated by 10° (see Figure 2 for a global view of the WEST divertor and the two probe arrays). The red curve is where the magnetic field line angle is maximum at the outboard side, and the blue curve is where the angle is maximum at the inboard side. The toroidal variation of angle is due to the toroidal field ripple which is large in WEST.

A domain of operation for the W-coated PFUs with the embedded LPs can be then derived using these profiles. It is seen that the narrowest heat loads pattern in the poloidal direction is for the far X-point configuration, which corresponds to the smaller flux expansion at the target plate. For the same reason, less SOL power is needed to obtain 10 MW/m^2 in the far X-point configuration because the heat flux is more focused. In this case, the deposited area covers poloidally a distance of ~8.5 cm at the inner divertor and ~6.5 cm at the outer divertor. The LPs were embedded at major radii corresponding to the centers of each future ITER-like MBs, therefore giving the probe array a spatial resolution of 12.5 mm. Therefore, such profiles shown in Figure 1 would present at least 7 and 5 measurement points at the inner and outer divertors,

respectively, which is sufficient for a good coverage of the profiles. Higher spatial resolution can be obtained by moderate sweeping of the strike points between two probes.

2.2 Probe design

Two arrays consisting of 29 flush-mounted LPs each are installed in the WEST flat, open divertor at toroidal angles 315° and 325° providing full poloidal coverage of the divertor wetted area. Due to the strong toroidal magnetic field ripple (7% [20]) introduced by the 18 superconducting toroidal field coils, the heat load pattern in WEST exhibits a n=18 toroidally periodic heat deposition pattern due to changing magnetic field incidence angles (the angle varies typically from 1° to 3°). The toroidal position of the maximum flux at the inner divertor corresponds to the minimum flux at the outer divertor because the vertical magnetic field from the toroidal field coils adds to or subtracts from the poloidal field associated with the plasma current, therefore the two arrays are separated toroidally by 10°, at locations corresponding to PFU#20 and PFU#32, in order to resolve both high flux regions. The LPs are embedded in special PFUs that are 50% wider than the standard ones to provide a volume that does not clash with the four legs used to attach the PFUs to the stainless steel support plate, to house the probes and to facilitate the cabling. Figure 2 shows a photograph of one of the probe arrays integrated into the WEST divertor. The special PFUs are beveled with an angle of 1° over the same toroidal width as the standard ones, and the extra zone around the probes is flat. Each PFU is divided into two parts covering the inner divertor on the HFS and the outer divertor on the LFS separated by a 0.5 mm toroidal gap in the private flux region. At the inner and outer strike point zones, the probes are mounted at the trailing edges of the PFUs, with respect to the direction of heat flow along the field lines. The LPs are poloidally spaced 12.5 mm apart in order to have the same spatial distribution as the W monoblocks constituting the ITER-like components of the future complete actively cooled WEST lower divertor. Each monoblock will be 12 mm wide and there will be 0.5 mm toroidal gaps between them, as foreseen in ITER [25].

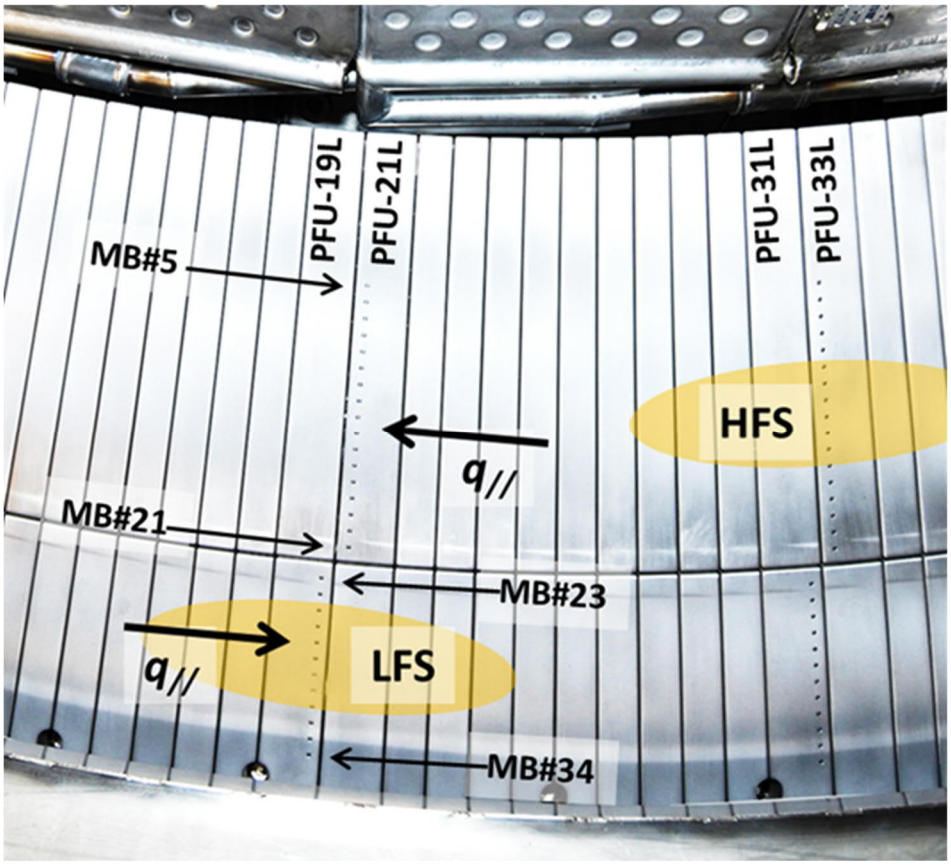

Figure 2. Photograph of the two pairs of wider diagnostic PFUs (19L & 21L and 31L & 33L) separated by 10° toroidally, where the flush-mounted LPs are embedded. The probes are numbered from MB05 to MB34 according to their positions with respect to the future actively cooled ITER-type monoblocks that will be installed in WEST Phase 2. There is no MB22 due to the presence of a 0.5 mm toroidal gap separating the HFS and LFS PFUs The direction of the parallel heat flux at the LFS and HFS regions is indicated.

As a design requirement within a full-metal tokamak, the LPs could not be made of graphite and had to be metallic. Tantalum (Ta) was preferred to stainless steel (SS), W, or molybdenum because it is a dense and hard material but also ductile and easily machinable at room temperature. It is a metal with relatively good heat and electrical conductivity and has a melting point around 3000 °C, which make it an ideal candidate for a diagnostic to be sitting in the harsh environment of long pulse tokamaks. Figure 3 shows the final design drawing of the LPs embedded in the PFU. Each LP tip is 2.5 mm in diameter (at the plasma side). Electrical insulation from the PFU is made using boron nitride rings and the probe is fixed by compression using a graphite M10 screw.

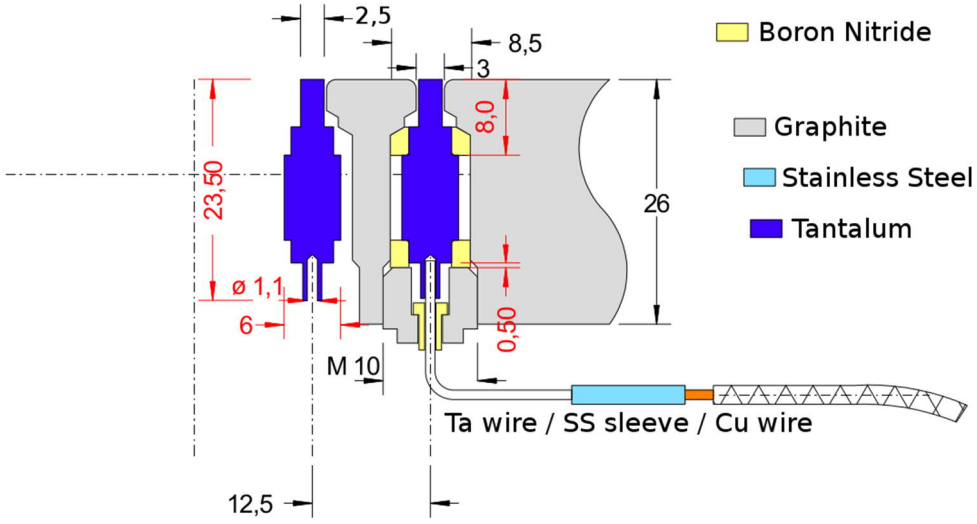

Figure 3. Schematic of the WEST divertor flush-mounted LP with dimensions in mm.

In order for the short circuit ion current theory to be applicable, the probe tips must be extremely well aligned with the PFU surface [26]. The alignment should be of the order of the ion Larmor radius so that the ion current collected by the probe when biased to the same potential as the target (zero volts) is a true measure of the local current that would flow to the target in the absence of the probe. At the WEST divertor, with B=4 T, T_i=1 eV, the deuteron Larmor radius is r_L=50 µm. An alignment of ±20 µm was sought. To achieve this, the Ta probes were manufactured to be a bit recessed 0.1±0.1 mm below the PFU surface. Before installation, an altitude map of the probes' recessions below the PFU surface was made by confocal microscopy (see Figure 4). An average value of -69±65 µm was obtained. In cases when the recession was deeper than -20 µm, the upper boron nitride ring was sanded delicately by rubbing it on emery cloth until the top of each Ta pin seemed flush with the PFU, which had already been coated with 15 µm of W. The human finger is extremely good at detecting small differences in surface relief [27]. The alignment of the pins was then measured by a second round of confocal microscopy to be 16±22 µm (see Figure 4). The value ±22 µm corresponds to the standard deviation of the distribution of the misalignments. The majority of the probes protrude slightly above the surface target. The largest measured misalignment is 75 µm. A few probes are recessed but only one is deeper than the 20 µm that were sought (its measured recession is -33 µm).

During long discharges, the entire probe body can reach temperatures higher than the copper (Cu) and SS melting points, 1085ºC and ~1450ºC, respectively, as observed during high heat flux tests (see Section 2.3). Therefore, to prevent failure of the electrical connection to each probe, a short length of Ta wire was crimped into the small tube at the bottom (Figure 3) of each probe. To ensure electrical insulation, a fiberglass braid was inserted around the Ta wire at the M10 screw interface. The Ta wire was joined to a shielded Cu wire by crimping a SS sleeve around both. The bundle of cables was pressed onto the PFU support plate by spot-welded collars. The support plate remains relatively cool even during long discharges and even if the PFUs themselves heat up to ~1000 °C, the heat they radiate towards the support plate is

not enough to damage the cables. Photographs of the connection method are shown in Figure 5.

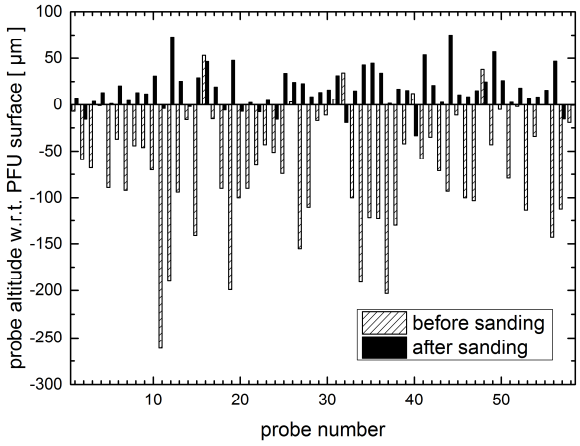

Figure 4. Altitude of each probe with respect to the PFU before (hashed bars) and after (full bars) manual sanding of the boron nitride insulation rings.

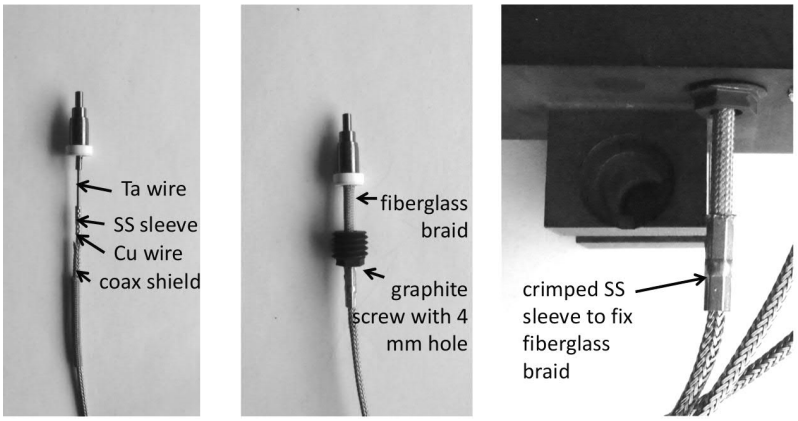

Figure 5. Photographs of the electrical connection scheme.

2.3 High heat flux tests in GLADIS

Before production and installation in WEST, the LPs were tested in the high heat flux (HHF) test facility GLADIS [21] where the mock-ups were adiabatically loaded with a Gaussian (~150 mm FWHM) hydrogen neutral beam. Two probe prototypes at scale 1:1 were manufactured and inserted in a graphite PFU mock-up representative of the WEST diagnostic PFU. Originally the LPs had a different preliminary design consisting of a SS base into which was screwed a threaded graphite probe tip, and to which a Cu wire was directly crimped. This preliminary design can be seen in Fig.4 of reference [18]. During a first HHF tests campaign [18], two scenarios were tested: (1) 10 MW/m^2 with 3.5 s loading and (2) 3.5 MW/m^2 with 40 s loading. The LPs behaved well under scenario (1) for which it was designed based on predictive thermal simulations, which represents intense but short loads with the temperature of the probe bases remaining always below 400°C even though the surface of the LPs graphite tips reached 1800°C. Under the long pulse, low power scenario (2) the absorbed heat was nearly 4 times

higher compared to the short pulse scenario, sufficient to melt the SS base. Therefore, in order to improve the thermal behaviour and to fulfil the requirement of a metallic LP tip, the probe design was changed to the present one completely made of Ta avoiding the SS base.
In a second HHF tests campaign in GLADIS, three Ta probes embedded in a W-coated graphite PFU mock-up were tested. This mock-up was representative to the final WEST diagnostic PFU design with the applied W coating technology [28]. The PFU mock-up was loaded at two positions to simulate the expected thermal loads at the two divertor strike-points in WEST. The experimental arrangement of the second HHF tests is shown in Figure 6 where the three Ta probes are marked with blue dots.

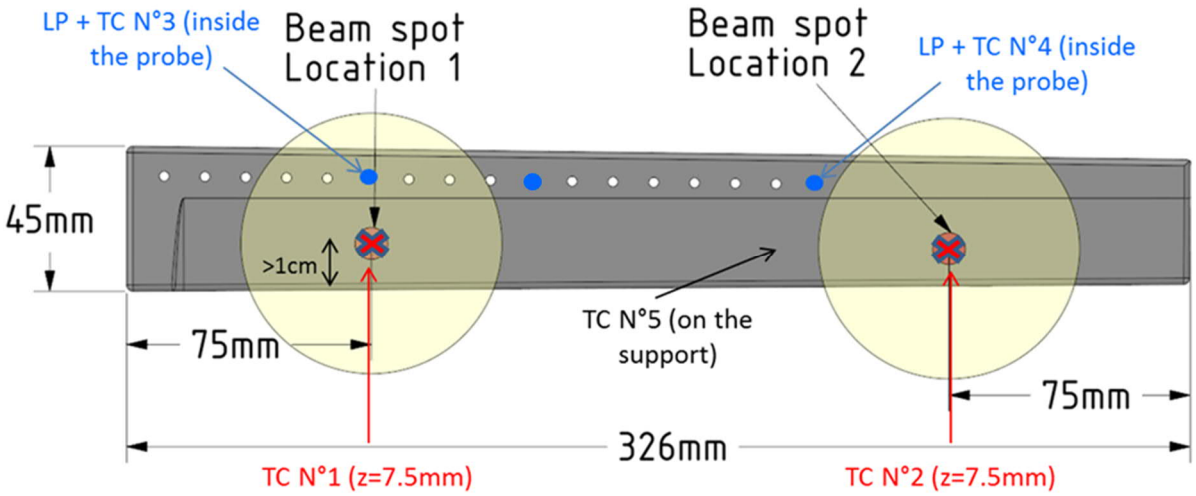

Figure 6. HHF tests configuration of three Ta LPs embedded in the W-coated graphite PFU mock-up and instrumentation (top view).

Two scenarios were performed similar to the first HHF test campaign:

(1) Short pulse, high power scenario; one pulse at 8 MW/m^2, 5.5 s loading, followed by 20 cycles 8 MW/m², 1.9 s loading every 60 s.

(2) Long pulse, low power scenario; one pulse at 5 MW/m^2, 6 s loading, followed by 20 cycles 5 MW/m², 1.9 s loading every 60 s followed by a final pulse at 3.5 MW/m², 40 s loading.

Three independent measurement systems recorded the thermal behaviour of the mock-up during the tests: one infrared camera (IR), a two-colour pyrometer, and 5 thermocouples (TC). Two of the TC were inserted in the graphite 7.5 mm below the surface at the two beam spot positions (TC 1,2) and the other two were directly inserted in two of the Ta probes (see Figure 6), crimped at their bottom (TC 3,4). The fifth TC was connected to the PFU support in between the two beam positions (TC 5). The main results are summarized in Table 1. Even though TC 3,4, measuring the probes base temperature, were saturated for the more problematic long pulse, low power scenario, no damage nor melting was observed post-exposure.

Loading	**Max. T_{surf} beam spot**	**T_{surf} graphite (TC 5)**	**T_{base} LP (TC 3,4)**
3.5 MW/m², 40 s, one pulse	1700 °C	> 1000 °C [1)]	> 1000 °C [1)]
5 MW/m², 6 s, one pulse	1020 °C	650 °C	460 °C
5 MW/m², 1.9 s, 20 cycles	1300 °C	> 1000 °C [1)]	865 °C
8 MW/m², 5.5, one pulse	1560 °C	900 °C	655 °C
8 MW/m², 1.9 s, 20 cycles	1650 °C	> 1000 °C [1)]	> 1000 °C [1)]

Table 1. Summary of the HHF tests of the Ta probes. The surface temperature at the beam spot was measured with a two-colour pyrometer. The upper limit of the data acquisition of the TC is marked by [1)].

As an example for the short pulse, high power scenario, the surface temperature distribution at the end of the 8 MW/m², 5.5 s pulse is shown in Figure 7a. Two of the three Ta LPs, inserted in the holes no.6 and no.10 (counting from left) are clearly visible in the IR image. However, no reliable surface temperature of the Ta tips could be measured due to the limited spatial resolution of the IR camera, the influence of the black body radiation from the holes and the undefined emissivity of the Ta tips. Figure 7b shows the temporal evolution of the surface temperature measured by the two-colour pyrometer and the temperatures of the two TC at beam location 1 for the same pulse. The maximum temperatures reached at the PFU surface (1560°C) and importantly at the probe base (655°C) are well below the Ta melting point. The loaded part of the mock-up reached its maximal equilibrium temperature about 25 s after loading.

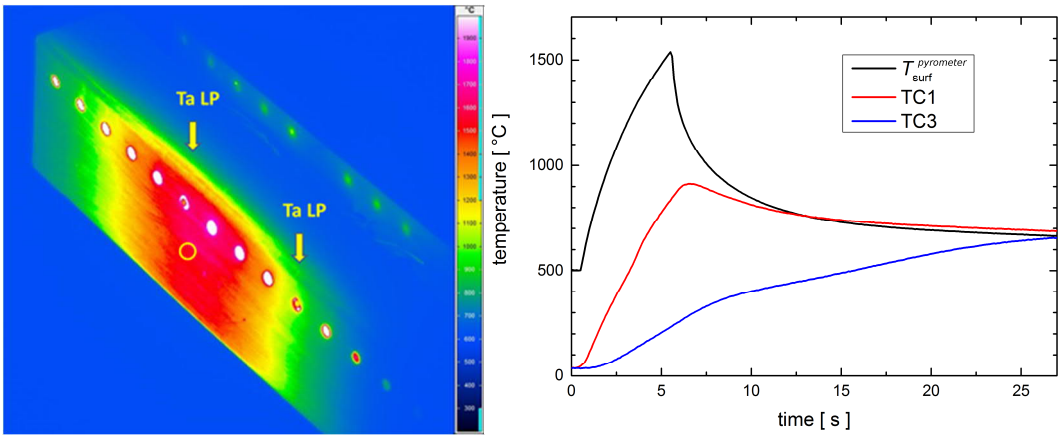

Figure 7. a) IR image at the end of the 8 MW/m², 5.5 s loading. The temperature scale ranges from 200°C to 2000°C. Two of the LPs, inserted in holes no.6 and no.10 (from left), are clearly seen and marked with arrows. The yellow circle marks the beam centre and the corresponding pyrometer spot. Thermal reflexions of the holes on the steel support are visible in the background. b) Temporal temperature evolution of the W-coated mock-up: surface temperature, pyrometrically measured (black), Ta LP 1 base temperature (at the beam spot location 1 in Figure 6) measured by TC 3 (blue) and temperature of the surrounding graphite mock-up measured by TC 1 (red) during the 8 MW/m², 5.5 s loading scenario.

This second series of tests was successful and validates the Ta probe design and also confirms the good quality of the W coating on the graphite PFU, validating again the overall design of the modified PFU.

3 First results

The WEST divertor probe system was commissioned and operational for the first discharge in WEST in 2016 (shot number 50000). The probes are swept from -200 V to +50 V for 1 ms, every 4 ms, and the collected *I-V* characteristics are analyzed as in [26] to provide quantities such as the local parallel ion current density ($J_{//,i}$), n_e, T_e, and the parallel heat flux

($q_{//}$). In the example shown in Figure 8 (shot number 55481), the plasma parameter profiles at the outer strike point were measured during a scan of X-point height from 55 to 85 mm, corresponding to a radial excursion on the target from R=2.237 to 2.277 m. The plasma current was I_p=500 kA, the line-averaged density was n_e=4.0×10^{19} m^{-2}, with lower hybrid heating power of P_{LH}=2.0 MW.

Despite slight differences in the alignment of neighbouring probes, uncertainties in the magnetic flux surface reconstruction and the possibility that the divertor plasma changes during the strike point sweep, the parameters measured by each probe overlap quite well. This is certainly a result of the effort to obtain alignment within ±20 µm, meaning that all the probes can be reasonably assumed to be geometrically identical. The profiles of parallel ion current density, electron temperature, parallel heat flux, and electron density peak at the separatrix (d_{sep}=0) and show sharp decays into the private flux region, and slower decays into the SOL. In this case the SOL heat flux decay length is λ_q=14 mm mapped to the outboard midplane. This value is larger than that deduced from infrared measurements [29] and closer to values measured by fibre Bragg gratings that exhibit values 3 times larger than infrared [30]. These differences are under investigation. At the separatrix the floating potential has a narrow, negative well. There is also an abrupt change in all the profiles at the outermost positions, which lie under the magnetic shadow of the baffle.

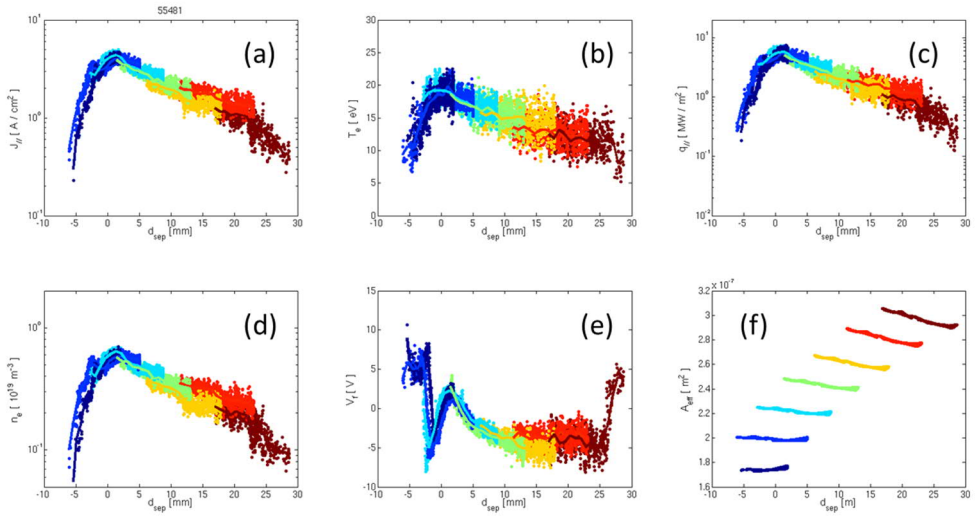

Figure 8. Plasma parameters measured at the outer strike point under the maximum of the toroidal ripple on shot 55481: (a) parallel ion current density; (b) electron temperature; (c) parallel heat flux; (d) electron density; (e) floating potential; (f) probe collecting area taking into account the local magnetic field angle. The strike point was swept 4 cm across the target, allowing to overlap the measurements from 3 probes. Results are plotted as a function of distance from the separatrix mapped to the outboard midplane. Each colour represents a different probe.

4 Conclusions

The Langmuir probe system for the WEST phase I, uncooled W-coated graphite lower divertor consists of W-coated tantalum tips, which are very well aligned with the tile surface in which they are embedded (16±22 µm) in order to withstand the high expected heat fluxes.

Tantalum metal was chosen because of its high melting point, and ductility at room temperature that allows simple crimping to electrically connect them to cables, as well as being compatible with the full metal environment of WEST. Two arrays of 29 probes cover the entire poloidal extent of the divertor region from HFS to LFS, separated toroidally by 10^{o} in order to study the effect of the strong toroidal field ripple modulation. The spatial resolution of 12.5 mm corresponds to the poloidal width of future tungsten ITER-like, actively cooled monoblocks of the WEST phase II divertor. The entire probe system, including the boron nitride insulators, the graphite fixing screws with fiberglass braid to ensure electrical insulation, and the Ta-Cu wire connections, was designed before the first diverted discharge, to withstand 10 MW/m^2 at the target. High heat flux tests performed in the neutral beam facility GLADIS confirmed the robustness of the design for fluxes up to 8 MW/m^2 for 5.5 s, and for 40 s long discharges at lower power densities (3.5 MW/m^2). The WEST flush-mounted divertor probe system was commissioned and operational since the first discharge in WEST in 2016. Measurements during a 4 cm strike-point sweep across the outboard target in order to increase the spatial resolution shows a very satisfactory overlap of plasma parameters measured by each adjacent probe, demonstrating the good alignment with the surrounding surface. The flush-mounted probes successfully measured in a wide range of operating conditions providing useful feedback in anticipation of ITER probe system. All the probes are fully operational after 3000 plasma discharges corresponding to 22000 seconds of plasma with a total of 1.5 GJ of additional RF heating power.

Acknowledgement

This work has been carried out within the framework of the project COMPASS-U: Tokamak for cutting-edge fusion research (CZ.02.1.01/0.0/0.0/16_019/0000768) and co-funded from European structural and investment funds and MEYS project LM2018117.

References

[1] M. Chatelier, Nucl. Fusion **47**, S579 (2007).

[2] J. Bucalossi, M. Missirlian, P. Moreau, F. Samaille, E. Tsitrone, D. van Houtte, T. Batal, C. Bourdelle, M. Chantant, Y. Corre, et al., Fusion Engineering and Design **89** (2014) 907-912

[3] Y. Corre, G. Laffont, C. Pocheau, R. Cotillard, J. Gaspar, N. Roussel, M. Firdaouss, J.-L. Gardarein, D. Guilhem and M. Missirlian, Review of Scientific Instruments 89 (2018) 063508

[4] J. Gaspar, Y. Corre, M. Firdaouss, J.L. Gardarein, J. Gerardin, J.P. Gunn, M. Houry, G. Laffont, T. Loarer, M. Missirlian, et al., Fusion Engineering and Design 146 (2019) 757-760

[5] M. Houry, C. Pocheau, M-H. Aumeunier, C. Balorin, K. Blanckaert, Y. Corre, X. Courtois, F. Ferlay, J. Gaspar, S. Gazzotti, et al., Fusion Engineering and Design 146 (2019) 1104-1107

[6] L. Chen, W. Zhao, G. Zhong, C. Watts, J. P. Gunn, X. Liu, Y. Lian and DLP Team, Fus. Sci. Tech. **73**, 568 (2018).

[7] Y. Jin, W. Zhao, C. Watts, J. P. Gunn, G. Zhong and X. Liu, Fus. Sci. Tech. **75**, 120 (2019).

[8] W. Zhao, Y. Wang, Y. Jin, L. Zhao, H. Zhou, L. Nie, G. Zhong, C. Liu, C. Watts and J. P. Gunn, Fus. Sci. Tech. **76**, 79 (2020).

[9] J. P. Gunn, C. Boucher, B. L. Stansfield and S. Savoie, Rev. Sci. Instrum. **66**, 154 (1995).

[10] M. Weinlich and A. Carlson, Physics of Plasmas **4**, 2151 (1997)

[11] A. Carlson, Phys. Plasmas **8**, 4732 (2001).

[12] D. Desideri and G. Serianni, Rev.Sci. Instrum. **69**, 2354 (1998).

[13] A. Bergmann, Phys. Plasmas **1**, 3598 (1994).

[14] A. Bergmann, Phys. Plasmas **9**, 3413 (2002).

[15] J. P. Gunn, C. Boucher, B.L. Stansfield, C.S. Maclatchy, Contrib. Plasma Phys. **36**, S45 (1996).

[16] J. P. Gunn, Phys. Plasmas **4**, 4435 (1997).

[17] J. G. Watkins, B. Labombard, P.C. Stangeby, C.J. Lasnier, A.G. McLean, R.E. Nygren, J.A. Boedo, A.W. Leonard, D.L. Rudakov, Journal of Nuclear Materials **463**, 436 (2015).

[18] M. Firdaouss, Y. Corre, P. Languille, H. Greuner, E. Autissier, C. Desgranges, D. Guilhem, J.P. Gunn, M. Lipa, M. Missirlian, et al., Phys. Scr. **2016**, 014012 (2016).

[19] A. Grosjean, Y. Corre, R. Dejarnac, J. Gaspar, J.P. Gunn, S. Carpentier-Chouchana, X. Courtois, E. Delmas, G. De Temmerman, M. Diez, et al., accepted manuscript in Nuclear Fusion (2020), https://doi.org/10.1088/1741-4326/ab9fa6.

[20] V. Basiuk, A. Becoulet, T. Hutter, G. Martin, A.L. Pecquet and B. Saoutic, Fusion technology **26**, 222 (1994).

[21] H. Greuner, B. Boeswirth, J. Boscary, P. McNeely, J. Nucl. Mater. **367–370**, 1444 (2007).

[22] Y. Corre, J. Gunn, B. Pegourie, R. Guirlet, C. De Michelis, R. Giannella, P. Ghendrih, J. Hogan, P. Monier-Garbet, A. Azeroual, et al., Nuclear Fusion **47**, 119 (2007).

[23] H. Bufferand, G. Ciraolo, Y. Marandet, J. Bucalossi, P. Ghendrih, J. Gunn, N. Mellet, P. Tamain, R. Leybros, N. Fedorczak, et al., Nuclear Fusion **55**, 053025 (2015).

[24] C. Bourdelle, J.F. Artaud, V. Basiuk, M. Becoulet, S. Bremond, J. Bucalossi, H. Bufferand, G. Ciraolo, L. Colas, Y. Corre, et al., Nuclear Fusion **55**, 063017 (2015).

[25] M. Missirlian, J. Bucalossi, Y. Corre, F. Ferlay, M. Firdaouss, P. Garin, A. Grosman, D. Guilhem, J. Gunn, P. Languille, et al., Fusion Engineering and Design, vol.**89**, no.7-8 (2014).

[26] J. P. Gunn, C. Boucher, D. Desroches and A. Robert, Rev. Sci. Instrum. **68**, 404 (1997).

[27] L. Skedung, M. Arvidsson, J.Y. Chung, C.M. Stafford, B. Berglund and M.W. Rutland, Sci. Rep. **3**, 2617 (2013).

[28] C. Ruset, E. Grigore, I. Munteanu, et al., Fusion Engineering and Design, vol.**84** (2014) 1662-1665.

[29] N. Fedorczak, J. Gaspar, M. Firdaouss, V. Moncada, A. Grosjean, R. Dejarnac, S. Brezinsek, E. Tsitrone, J. Bucalossi, T. Loarer and the WEST team, Phys. Scr. **2020**, 014046 (2020).

[30] N. Fedorczak, J. Gaspar, Y. Corre, A. Grosjean, X. Courtois, J.P. Gunn, R. Mitteau, R. Dejarnac, J. Bucalossi, E. Tsitrone, et al., Submitted to Nuclear Materials and Energy (2020).